Catalysis Today 148 (2009) 212–220

Contents lists available at ScienceDirect

Catalysis Today

journal homepage: www.elsevier.com/locate/cattod

Short review

Surface science perspective of carbon dioxide chemistry—Adsorption kinetics and dynamics of CO_2 on selected model surfaces

U. Burghaus *

Department of Chemistry, Biochemistry, and Molecular Biology, North Dakota State University (NDSU), Fargo, USA

ARTICLE INFO

Article history:
Available online 18 August 2009

Keywords:
CO_2 utilization
Surface science
Heterogeneous catalysis
Kinetics
Molecular beam scattering
Adsorption dynamics

ABSTRACT

The adsorption or formation of CO_2 on surfaces is important in a variety of industrial and environmental applications such as methanol synthesis, exhaust cleaning, CO_2 capturing/sequestering, fuel cell poisoning, fuel synthesis, etc. For most of these processes, a deeper understanding of the kinetics and dynamics of CO_2 adsorption on surfaces could help to optimize the performance of catalysts. Historically, most surface science studies have focused on CO rather than CO_2 as the probe molecule, i.e., fundamental knowledge about CO_2 adsorption is still needed. This paper will focus on summarizing a few fundamental properties of CO_2 adsorption on a number of selected model systems recently studied in our group. In particular, metals (Cu, Cr) and metal oxide (ZnO, TiO_2, CaO) single crystals as well as so-called model catalysts (Cu-on-ZnO, Zn-on-Cu) and nanocatalysts will be considered. The similarities and differences between metals and metal oxides will be highlighted as well as the effect of surface defects. An attempt to tie the different systems together by proposing structure–activity relationships rules will be made. Kinetics experiments and molecular beam scattering data are summarized, some of which have been modeled by Monte Carlo simulations and density function theory.

1. Introduction

What motivates a physicist, trained in traditional experimental surface science, to study CO_2 chemistry? Historically [1], surface science focused on metal single-crystal surfaces using CO as the probe molecule to gain a deeper understanding of the electronic, vibration, kinetic, and dynamic properties of surfaces. Well, CO_2 may be the next more complicated probe molecule. In addition to this pragmatic view (gaining better knowhow through the collection of larger data sets), there are numerous important applications that could stem from a deeper mechanistic understanding of the interaction of CO_2 with various surfaces. (1) Disregarding an initial controversy, the main source of carbon in the synthesis of methanol (MeOH) from syngas is CO_2 [2,3]. Thus, the adsorption of CO_2 on the catalyst surface is the first elementary reaction step in the sequence of hydrogenation reactions that lead finally to the formation of MeOH (Fig. 1). MeOH, obtained by utilizing CO_2, is an important feedstock in the chemical industry and can also be directly used as a fuel in direct liquid fuel cells. Recycling the greenhouse gas CO_2 from the atmosphere to build an economy based on MeOH has been proposed [4]. As a realistic model system for MeOH synthesis, the adsorption of CO_2 has been studied on clean ZnO single-crystal surfaces [5,6] as well as on Cu nanoparticles deposited on ZnO (Cu-on-ZnO) [7,8] by a variety of groups since industrially (among other systems) ternary ZnO-Al_2O_3-Cu powder catalysts are used. Our results (mostly kinetics and molecular beam scattering experiments) [5] are summarized in Section 4.2. Studying the effect of hydrogen and CO_2 coadsorption is the next logical step [9,10] (see Section 4.2.2). A related model system is bimetallic surfaces. Thus, Section 3 will discuss the work done on copper single crystals, and Section 5 considers ZnCu surface alloys using CO_2 as the probe molecule [11–13]. Alloy sites have been considered as the active sites in the synthesis of methanol. (2) Closely related to the venue of this conference is the geological sequestration of CO_2 as well as its capture in the exhaust gas of power plants (Fig. 2). Ca is used for the latter; and an interesting class of minerals, perhaps suitable for CO_2 sequestration, consists of Ca compounds [14]. Section 4.3 will summarize our studies of CO_2 adsorption on CaO(1 0 0) surfaces [15]. Regarding metal oxides, the effect of surface defects (oxygen vacancy sites) as well as the formation of surface carbonates are interesting mechanistic details. CaO is an excellent model system in this regard. A variety of further applications for CaO are known, including catalytic gasification of Ca-containing coal [16,17], NO storage catalysts used for operating combustion engines at lean (oxygen-rich) conditions with alkaline-earth oxides as promising catalysts, the capture of SO_2 by CaO [16], the dimerization of, for example, methane [18], the reduction of NO by CO [19], and the

* Tel.: +1 7012319742; fax: +1 7012318831.
E-mail address: uwe.burghaus@ndsu.edu.

0920-5861/$ – see front matter © 2009 Elsevier B.V. All rights reserved.
doi:10.1016/j.cattod.2009.07.082

Symbols and acronyms

SAR	structure–activity relationships
HAS	He atom scattering
AES	Auger electron spectroscopy
CNTs	carbon NT
DFT	density functional theory
FTIR	Fourier-transform infrared spectroscopy
HREELS	high-resolution electron energy loss spectroscopy
HOPG	highly oriented pyrolytic graphite
LEED	low-energy electron diffraction
MCS	Monte Carlo simulations
MIES	metastable impact electron spectroscopy
NEXAFS	X-ray absorption fine structure
NT	nanotubes
STM	scanning tunneling microscopy
TDS	thermal desorption spectroscopy
TiNTs	TiO_2 NT, inorganic NT
UPS	UV photoelectron spectroscopy
UHV	ultra-high vacuum
UV	ultra violet
XPS	X-ray photoelectron spectroscopy
T_s	adsorption temperature
α_i	impact angle
S_0	initial adsorption temperature
E_i	impact energy
Θ	coverage, surface particle density
$S(\Theta)$	coverage dependent adsorption probability

decomposition of chlorinated hydrocarbons [20]. For the decomposition of NO, CaO has been considered as a less expensive catalyst than systems based on noble metals [21]. Some work conducted on the prototype of a metal oxide, rutile TiO_2(1 0 0), will be summarized for completeness in Section 4.1; this discussion focuses on CO_2 adsorption [22,23]. (3) CO_2 is generated in the combustion of coal, which often includes inorganic impurities such as Ca and Fe (Fig. 3). Section 6.2 will discuss kinetics studies about CO_2 adsorption on Fe-oxide nanoparticles supported on HOPG as a model system for particulate matter that is released in the plume of coal combustion plants [24,25].

In addition to applications, as one motivation, surface science research on CO_2 aimed to address fundamental questions such as the following: (1) What are the fundamental differences in the catalysis of metal and metal oxide surfaces? How well can more complex surfaces be understood? (2) How do the adsorption kinetics and dynamics change when we go from a metal surface to a related metal oxide film [26]? (3) Is the adsorption kinetics

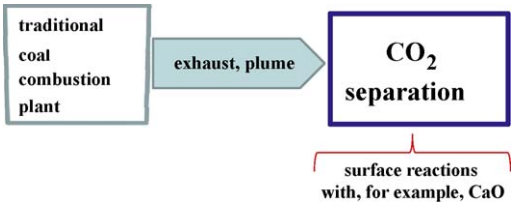

Fig. 2. CO_2 capturing.

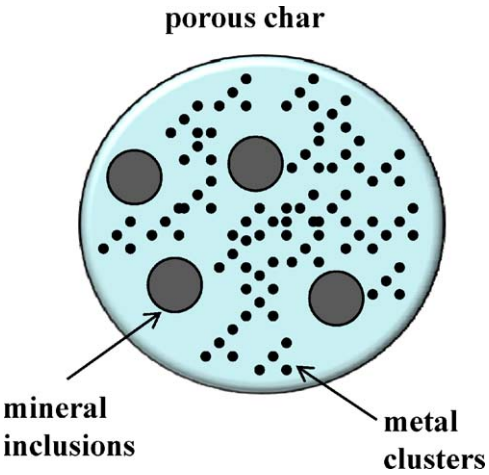

Fig. 3. Coal particle with inorganic impurities.

correlated in a simple way to the adsorption dynamics (gas-surface energy transfer processes)? For example, CO_2 binding energies on oxides are typically larger than for metal surfaces. What about adsorption probabilities governed by gas-surface energy transfer processes? (4) Oxide surfaces consist of very characteristic defects such as oxygen vacancy sites. How is the catalytic activity affected by these defects? Can we tune the reactivity of metal oxide surfaces by varying the defect density? Can these (model) defects serve to better understand powder catalysts or nanoparticles that have a large defect density? (5) How does the oxidation state of a system such as FeO_x affect the kinetics/dynamics of surface reactions? (6) How does the size (and shape) of supported metal (metal oxide) clusters relate to chemical activity? Again, a deeper understanding of the mechanism would allow for catalyst tuning, etc.

This mini review will mainly summarize the work done in 2004–09 at NDSU on CO_2 chemistry using molecular beam scattering and traditional kinetics techniques. Metal single crystals (Section 2), metal oxide films (Section 3) and single crystals (Section 4), bimetallic surfaces (Section 5), and nanostructured catalysts (Section 6) will be considered. The obtained results are discussed along with studies from other groups; however, due to

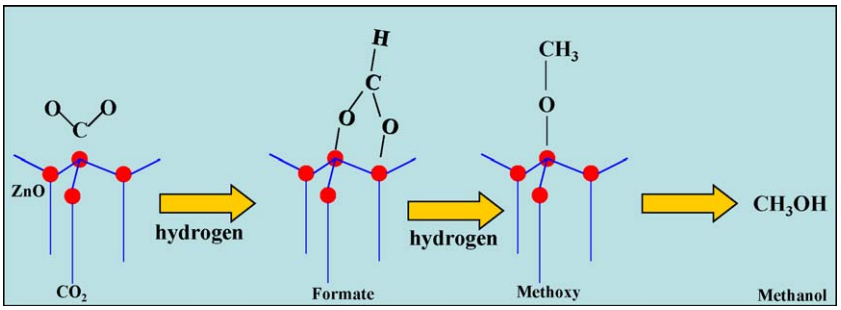

Fig. 1. Simplified reaction schematics for the synthesis of methanol [117].

strict text size limitations of the conference proceedings, for more complete surveys, see Refs. [27–31]. Similarly, details about experimental and theoretical techniques are omitted [32,33]. Very briefly, the first step in all surface reactions is the adsorption of at least one reactant on the catalyst. Molecular beam scattering allows understanding of the gas-surface energy transfer processes governing this adsorption process (referred to as adsorption dynamics). Thus, the potential energy surface can be mapped. Often complementary information is obtained by kinetics techniques such as TDS, a simple temperature ramping technique. Whereas TDS is a simple and readily available technique, molecular beam scattering systems are rather rare in the surface science community. This may be related to the fact that the equipment is not available commercially and that these multi-chamber UHV systems are somewhat more maintenance intensive.

2. Interaction of CO_2 with metal single-crystal surfaces—the case of CO_2/Cu(1 1 0)

2.1. Kinetics

CO_2 adsorption kinetics has been studied thoroughly on Cu(1 1 0) [34,35] and other metal surfaces (see e.g. Ref. [36]). Copper surfaces are prototypical due to the importance of Cu in the methanol synthesis which is one possibility to recycle CO_2. According to prior work, CO_2 desorbs at ~90 K in the monolayer range (see Table 1), obeying 1st order kinetics. Strong CO_2–CO_2 lateral interactions have been identified from TDS peak shifts [34] that lead to a continuous transition from monolayer to multilayer desorption peaks in TDS curves. Except for water adsorption, this effect has rarely been seen, and the very narrow width of TDS curves that amount only to 4 K is rather uncommon. In studies on powder samples as well as stepped Cu surfaces [37], the dissociation of CO_2 has been reported. DFT calculations [38] indicate that the reactivity toward CO_2 adsorption follows the commonly observed trend, Cu(1 1 0) > Cu(1 0 0) > Cu(111), which is in agreement with the coordination of the different crystallographic orientations.

2.2. Dynamics

Despite a large database about CO adsorption dynamics on a variety of systems [39–44], astonishingly few projects deal with the adsorption dynamics of CO_2 on metal surfaces [27,28]. We are aware of only one study, see Ref. [45]. That fact may simply be related to the rather small binding energies [46] compared with metal oxide surfaces [5,6,28], which renders experiments with CO_2 on most metal surfaces experimentally more difficult than those for CO. The modeling of related molecular beam scattering data of the Zn-on-Cu(1 1 0) system [13] requires, however, detailed knowledge about the interaction of CO_2 with clean copper surfaces. For Cu(1 1 0), the initial adsorption probability, S_0, is quite small and decreases exponentially from 0.43 to a value close to the detection limit (~0.05) within the accessible impact energy range [13]. S_0 is independent of T_s and α_i, i.e., the adsorption is non-activated, and total energy scaling (see Section 4.2) is obeyed. At large temperatures, the coverage dependent adsorption probability, $S(\Theta)$, agrees with precursor-assisted adsorption dynamics—the molecule is trapped above occupied sites before adsorption on clean surface sites takes place. However, at lower surface temperatures, adsorbate-assisted adsorption (S increases with Θ) has been observed. This is a typical adsorption scenario, except for the very narrow temperature range where the adsorption dynamics shows a cross-over from adsorbate-assisted (S increases with Θ) to Kisliuk-like ($\Theta \sim$ const) behavior (Fig. 4). The adsorbate-assisted adsorption effect may be considered as an analog to an autocatalytic reaction. The efficiency of the energy transfer in gas-surface collisions should be related to the corresponding mass match. The matching of projectile and target masses is certainly perfect for trapping CO_2 molecules above already adsorbed CO_2 and is less favorable for CO_2-surface collisions. The probability for the first event is proportional to the coverage, i.e., S increases naturally with Θ. In addition an interesting feature is seen for the Cu system. The adsorbate-assisted adsorption effect is only dominant at large coverages of the surface species. With increasing temperature the saturation coverage decreases which generates a cross-over from adsorbate-assisted (at low temperature and high coverage) to Kisliuk adsorption dynamics (at lower coverage and greater temperature).

3. Metals vs. thin oxide films—the case of Cr(1 1 0) vs. Cr_2O_3(0 0 0 1)

In this project, we compared directly the chemical activity of a metal surface and its surface oxide toward CO_2 adsorption [26]. The Cr(1 1 0) surface can simply be distinguished from the Cr_2O_3(0 0 0 1) surface oxide by the appearance of a square or hexagonal LEED pattern, respectively, as well as by TDS curves consisting of a single or double peak. The latter is consistent with an oxygen-terminated oxide surface [47]. At low temperatures, CO_2 physisorbs on both surfaces. S_0, is for both systems independent of T_s and decreases exponentially with increasing impact energy. Therefore, non-activated adsorption is concluded, and precursor-mediated adsorption with a trapping probability which decreases as E_i increases.

The surface oxide is more reactive than the metal toward CO_2 adsorption judging by the binding strength of the probe molecule (Table 1). However, S_0 is systematically smaller for the oxide compared with the metal. In some cases, considering simply the gas-to-surface mass match is very successful in explaining trends

Table 1
Kinetics and dynamics parameters of CO_2 adsorption for the systems discussed. E_d denotes the heat of adsorption for pristine and defect sites. S_0 refers to the initial adsorption probability.

	System	E_d in kJ/mol pristine	E_d in kJ/mol defects	S_0	Ref.
Metals	Cu(1 1 0)	21.4	23.7	0.43	[13]
	Zn-on-Cu(1 1 0)	<21		0.45	[11]
	Cr(1 1 0)	33.3		0.69	[26]
Metal oxides	ZnO	34.4	43.6	0.73	[5–10]
	TiO_2	43	48	0.56	[22,23]
	CaO(0 0 1)	28 → 80		0.60	[15,25,119]
	CrO_x-on-Cr(1 1 0)	30.5	39.5	0.58	[26]
Nanostructures	Cu-on-ZnO	26	40	0.4	[7,8]
	FeO_x-on-HOPG	33 → 48		0.7	[24]
	TiO_2 nanotubes	35			[110]

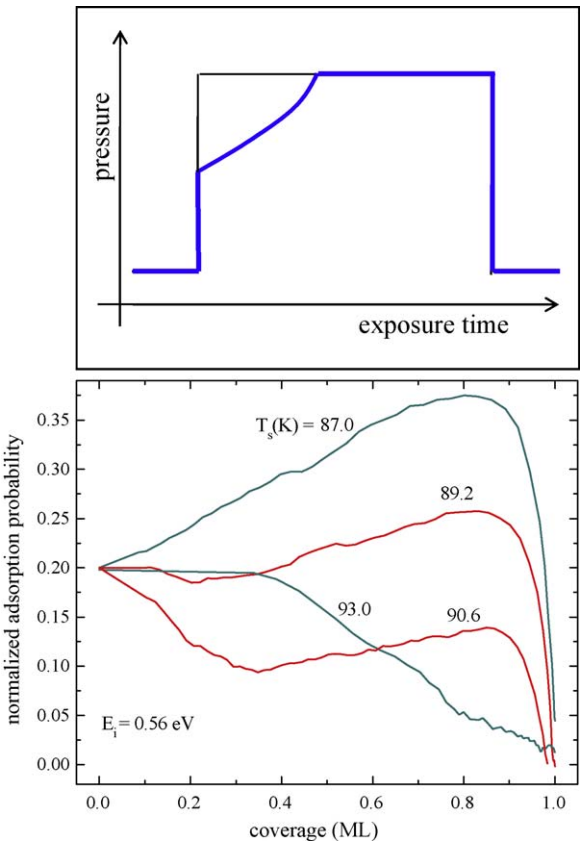

Fig. 4. (Top) Schematics of an adsorption isotherm experiment. Shown (thin line) is the beam profile (no adsorption) and the effect of a surface intercepting the beam (thick line). Integrating and normalizing these isotherms yield the coverage dependence of the adsorption probability. (Bottom) Coverage dependence of the adsorption probability of CO_2 on Cu(1 1 0). The cross-over from adsorbate-assisted adsorption (S increases with coverage) to Kisliuk adsorption dynamics ($S \sim$ const) is observed within a very narrow temperature range [13].

observed experimentally. The matching of the CO_2 to Cr masses (44/52 = 0.85) is better than the one for CO_2 and oxygen (44/16 = 2.75). Although metal and metal oxides have certainly different electronic structures, considering the simple mass-matching model S_0 for the O-terminated surface oxide should be smaller than for Cr(1 1 0), as indeed is observed. However, comparing a larger data set does not lead to a fully consistent picture [48]. Therefore, static and dynamic corrugation effects [49,50] as well as the effect of lateral interactions have been considered. For both systems and as commonly observed, the coverage dependence of the adsorption probability is, at low E_i, independent of coverage (Kisliuk-shape) and $S(\Theta)$ increases initially with coverage (adsorbate-assisted adsorption) at large E_i, indicative of precursor-mediated adsorption. The adsorption dynamics have been modeled by MCS [51].

4. Interaction of CO_2 with metal oxide single crystals

4.1. CO_2 adsorption on rutile TiO_2(1 1 0)

4.1.1. Surface defects and kinetics

Rutile TiO_2(1 1 0) is the prototype of a metal oxide model system [52]. In particular, surface defects on TiO_2(1 1 0) have attracted the interest of many research groups [53–55] since defects are often the active sites in catalytic processes. However, creating defects in a well-controlled manner is challenging: sputtering [6,56,57], electron or UV exposure [58], reduction with hydrogen or CO [59], and annealing above 600 K have been used. It is believed that ion sputtering removes preferentially surface oxygen. As initially shown by Henderson [55], Yates [54], et al., CO_2 is a perfect probe molecule to quantify the effect of oxygen vacancy sites on TiO_2(1 1 0) by TDS. A single CO_2 TDS peak appears on the oxidized surface [54,55] that was assigned to adsorption on fivefold coordinated Ti^{4+} sites. Annealing in UHV resulted in a second high-temperature TDS peak, assigned to adsorption on Ti^{3+} oxygen vacancy sites [54]. According to an HREELS study [55], CO_2 adsorbs molecularly in linear geometry on Ti^{4+} sites; adsorption geometry on defect sites has not been identified for single crystals. Measurements on powders and theoretical studies [60] suggest, however, bent CO_2^- species exist on the oxygen vacancy sites of metal oxides. Even the oxidized surface consists, according to STM results [61], of ~10% oxygen vacancy sites. Please note that oxygen vacancy sites can be readily hydrogenated by H_2O uptake from the residual background gas [61,62].

4.1.2. Molecular beam scattering (adsorption dynamics)

Molecular beams use neutral probe particles, i.e., this technique is particularly well suited for studying less conducting samples. However, astonishingly, only a very few studies have characterized the gas-surface energy transfer processes for metal oxide surfaces. Molecular beam scattering experiments with CO_2 on metal oxides have, to the best of our knowledge, been conducted only by our group. For example, we studied the adsorption dynamics of CO_2 on rutile TiO_2(1 1 0) as a function of E_i, T_s, hydrogen, and oxygen preexposure, as well as the density of defects as varied by annealing and Ar^+ sputtering [22,23]. S_0 decreases linearly with E_i and is independent of T_s. The adsorption dynamics are dominated by the effect of precursor states leading to Kisliuk-like $S(\Theta)$ shapes over the E_i and T_s range studied. The shape of the $S(\Theta)$ curves was essentially independent of the defect density. Interestingly, oxygen vacancy sites reduce the initial activity (i.e., S_0) of the surface toward CO_2 adsorption. Pre-adsorbed oxygen preferentially blocks defects sites, which leads again to an increase in S_0. Thus, the oxygen vacancy sites heal out. Hydrogen preadsorption results in a physical site blocking with S_0 decreasing with preexposure. In contrast to oxygen, hydrogen does not preferentially adsorb on defect sites. In summary, the catalytic activity of this model system can be tuned in principle by controlling the surface defect density.

4.2. CO_2 adsorption on clean and hydrogen covered ZnO and the effect of defects

4.2.1. Surface structure

The Zn-terminated ZnO surface, ZnO(0 0 0 1), is characterized by a bulk terminated (1 × 1) structure, as evident from HAS [62] and most LEED [63] studies. In addition, STM measurements presented evidence of distinct defect structures [63,64], which lead to the electrostatic stability of the polar Zn–ZnO surface. HAS data suggest the formation of a (1 × 1) H overlayer by dosing hydrogen or water [65–67] on ZnO. However, extensive exposure of atomic hydrogen results in a breakdown of the surface, leading to the formation of hydroxyls.

4.2.2. Adsorption kinetics

Chemisorption of CO_2 well above room temperature has been thoroughly studied on ZnO surfaces [68–73]. Physisorption of CO_2 on ZnO surfaces has been studied in less detail [74]. Similarly to kinetics studies conducted on TiO_2, for ZnO the effect of surface defects is nicely seen in TDS experiments (Fig. 5) [5,6]. Two TDS structures are evident. Preexposing hydrogen leads to the disappearance of the high-temperature feature whereas sputtering increases the intensity of this peak. Thus, the high-temperature TDS peak is assigned to CO_2 adsorption on defect sites, and the

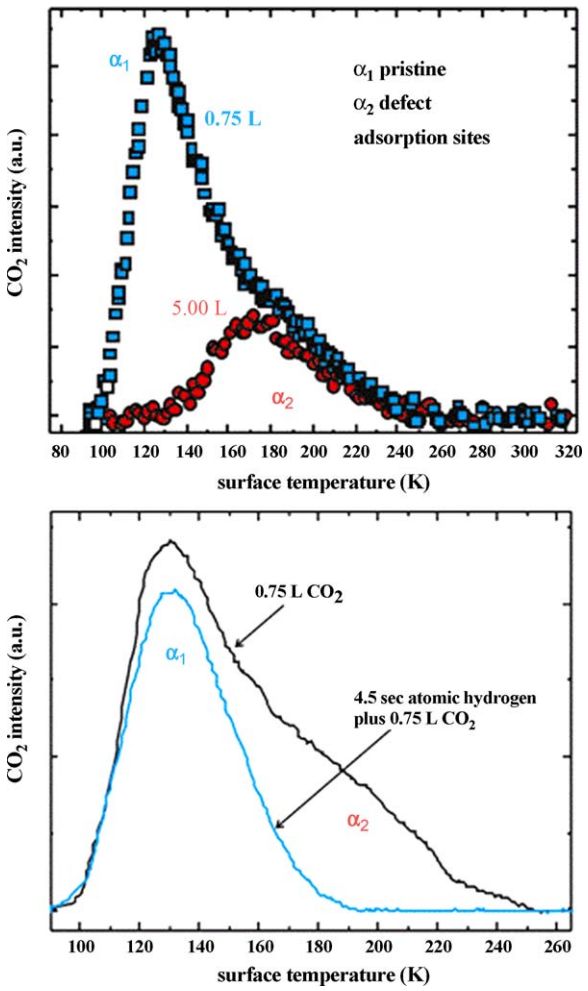

Fig. 5. (Top) CO_2 TDS (thermal desorption spectroscopy) on ZnO(0 0 0 1). At low exposures, only high-energy binding sites (defects) are populated (α_2 peak). With increasing exposure, pristine sites (α_1 peak) are also covered by CO_2. (Bottom) Hydrogen preferentially adsorbs on defect sites. Thus, preadsorbing hydrogen suppresses the defect peak in subsequent CO_2 TDS experiments [6].

low-temperature peak corresponds to CO_2 decorating pristine sites on the ZnO(0 0 0 1) surface.

4.2.3. He atom thermal desorption spectroscopy

The effect of surface defects can be studied in an elegant way using molecular beam scattering techniques [75]. The cross-section for diffuse HAS on defects is very large. Thus, the specularly backscattered He atom signal solely samples the pristine sites on the surface. In contrast, measuring adsorption isotherms (i.e., adsorption probability curves) results in data representing an average of all available adsorption sites. Using seeded beams (He mixed with CO_2) and detecting He reflectivity and CO_2 adsorption probability curves simultaneously allows the effect of defects and the adsorption dynamics to be characterized in a single experiment. A typical result is shown in Fig. 6. The adsorption probability curve indicates saturation of the surface with CO_2 obeying traditional precursor dynamics. However, the expected decay of the He atom signal with CO_2 exposure (the thin line in Fig. 6 calculated for a cross-section of 100 $Å^2$) should be much faster than detected. Thus, the CO_2 molecules adsorb preferentially on defect sites and remain therefore invisible for the backscattered He atoms. Therefore, the He signal decays slowly. When terrace sites also start to fill up with CO_2, the He signal starts to drop. The combination of adsorption probability measurements and HAS

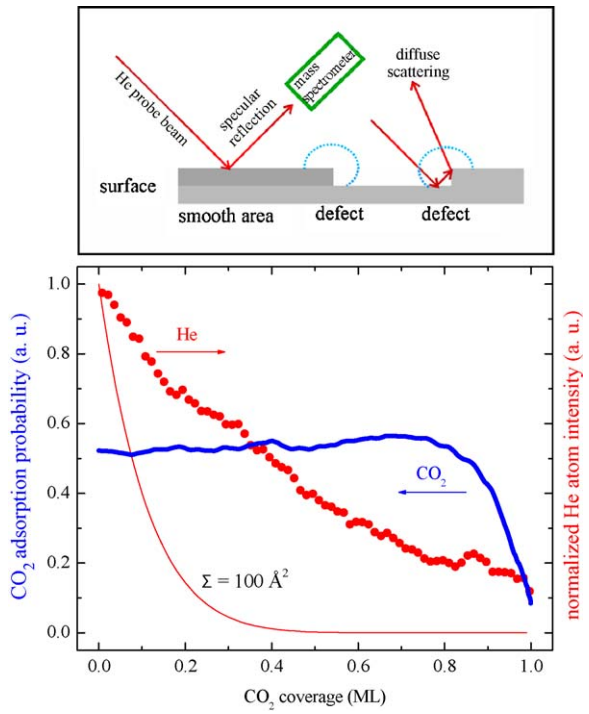

Fig. 6. (Top) The specularly backscattered He atom intensity samples the clean and defect-free areas of the surface. (Bottom) Combination of adsorption transients and He atom reflectivity curves using seeded beams (CO_2 in He) [9].

unequally reveals preferentially adsorption of CO_2 on defect sites. This type of experiment can also be performed while ramping the surface temperature: He atom TDS [76].

4.2.4. Cooperative precursor effects

Uncommon adsorption dynamics have been seen for CO_2/ZnO at large impact energy [5]. The shape of $S(\Theta)$ deviated from the simple Kisliuk model: $S(\Theta)$ remains initially constant and then starts to increase before the surface saturates and $S(\Theta)$ drops naturally to zero (Fig. 7). In the traditional Kisliuk model, as well as in related MCS [77–79], trapping of a particle in an extrinsic precursor state requires solely that the point of impact be occupied. In other words, one adsorbed molecule already defines the precursor state. Clearly, critical coverage of CO_2 on the surface is required before S starts to increase with Θ (Fig. 7). A model consistent with these findings assumes a "cooperative" precursor

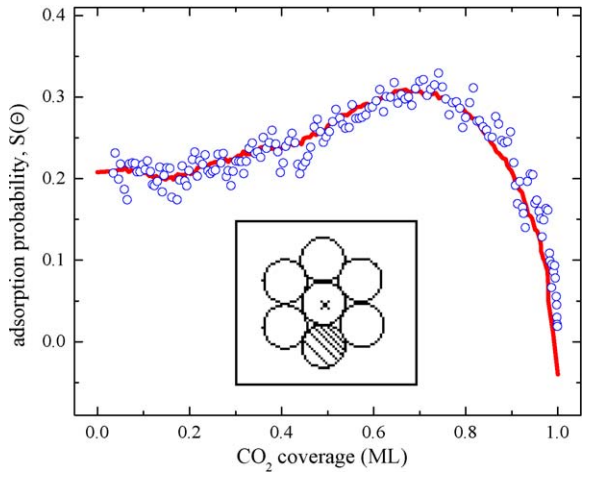

Fig. 7. Cooperative precursor effects—CO_2 adsorption on ZnO(0 0 0 1) [5].

effect [48]: at least one nearest neighbor site (see the hatched sphere in the inset of Fig. 7) that is adjacent to the point of impact (labeled by the cross) needs to be occupied for successful trapping of the molecules in the extrinsic precursor state. This cooperative effect suppresses initially trapping in the precursor state and reproduces the bimodal shape observed experimentally. The result of the corresponding MCS is depicted as a solid line in Fig. 7.

4.2.5. Mapping the potential energy surface

Understanding the details of gas-surface energy transfer processes requires understanding how the parallel and normal components of the momentum of the gas-phase species affect the reactivity of the system. In other words, how does S_0 depend on the impact angle? In addition, how do internal degrees of freedom (vibrations, rotations) of the projectile affect surface reactions? For example, vibrational excited alkanes break down when adsorbed on the CaO surface [80].

The simplest impact scenario would predict total energy scaling in the case of rather rough metal oxide surfaces; i.e., S_0 should be independent of the impact angle; $S_0(E_i, \alpha_i) \sim S_0(E_i, 0^\circ)$. For less-corrugated surfaces, however, normal energy scaling [50,81], which obeys $S_0(E_i, \alpha_i) \sim S_0(E_i \cos^n(\alpha_i), 0^\circ)$ with $n = 2$, should be observed. Smaller n values indicate generally an effect of parallel momentum of the gas-phase species on the energy transfer processes. Intermediate cases with $1 < n < 2$ [82] may be caused by an interplay of different energy transfer mechanisms that dominate the adsorption dynamics in different impact energy ranges. For example, the magnitude of the barrier height for activated adsorption might vary along the surface (“energetic corrugation”) or the barrier height may remain constant, but local variations of that barrier might appear (“geometric corrugation”) [83].

$S_0(\alpha_i)$ curves obtained for ZnO(0 0 1) along the [0 0 1] azimuth direction, parametric in E_i, but for a constant temperature, show a small dispersion. S_0 is independent of α_i for $E_i < 0.56$ eV. However, above that threshold, S_0 starts to decrease slightly with α_i.

Anisotropy effects in S_0 were more distinct for CO adsorption on TiO_2(1 1 0) due to the large surface corrugation. Although a decrease in S_0 with α_i has indeed been observed at large E_i, along both high symmetry azimuth directions approx. identical numerical values of S_0 have been determined. Interestingly, for large E_i approx. normal energy scaling is obeyed along both high symmetry azimuth directions. However, total energy scaling at low impact energies. Those results point to an interplay of energetic and geometric corrugation effects, respectively. Therefore, normal energy scaling can also be observed for highly corrugated surfaces.

Most of the models briefly described above focus solely on S_0. However, the whole shape of adsorption probability curves can also be distinctly influenced by surface corrugation. For example, in the case of CO_2 adsorption on ZnO(0 0 0 1), the adsorbate-assisted adsorption effect disappears as the impact angle increases. Or, for CO/TiO_2(1 1 0) and along the highly corrugated [1–10] azimuth, adsorbate-assisted adsorption has been observed and was most distinct at glancing angles of incidence; however, along the less-corrugated [0 0 1] azimuth direction standard precursor-mediated adsorption ($S \sim$ constant) was present [84]. For CO/Cu(1 1 0), a system that also shows the adsorbate-assisted adsorption effect [42], however, the impact angle hardly influences the shape of $S(\Theta)$.

4.3. CO_2 adsorption on alkaline-earth oxides—the case of CaO(1 0 0) and the formation of carbonates

A possible formation of surface carbonates (adsorbed CO_3) at UHV conditions is a long-standing topic of studies on metal oxide surfaces. Carbonate formation has been proposed for a number of (oxygen-terminated) metal oxide surfaces (including ZnO and Cr_2O_3), often with somewhat conflicting evidence. A perfect model system in this regard is the catalytic highly active CaO metal oxide.

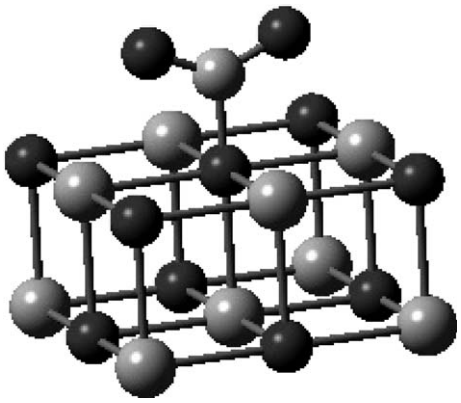

Fig. 8. Carbonate formation involving lattice oxygen [15].

CO_2 adsorption on CaO leads, according to XPS and NEXAFS data, to the formation of CO_3^{ads}. In contrast to metal surfaces where carbonates form (in most cases thermally activated) in oxygen–CO or oxygen–CO_2 coadsorption phases, CO_3^{ads} formation on metal oxides can involve lattice oxygen (Fig. 8). For example, CO_2 chemisorbs on oxygen sites of the CaO(1 0 0) surface, yielding carbonate-like species [85]. Carbonates have also been detected in UPS and MIES experiments on CaO thin films [86,87]. For CaO powders, CO_2 desorption temperatures as high as ~1100 K have been seen, as the result of carbonate decomposition [16,88]. In an early IR study, the formation of bidentate and monodentate carbonates was proposed on powder samples. In this case, isotope scrambling indicated that surface oxygen is involved in the CO_3^{ads} formation [89]. The formation of carbonates on CaO has also been theoretically confirmed [90,91].

A comparison of CO_2 and CO adsorption is interesting. According to recent DFT calculations [15], CO does not adsorb on O-lattice sites. CO mainly adsorbs via the C-atom on Ca-sites. In contrast, the most stable adsorption configuration of CO_2 is via the C-atom adsorbed on O-sites of CaO, i.e., carbonate-like species form (Fig. 8). CO_2 does not adsorb either via the O-atom or on Ca-sites. Recent TDS experiments indeed revealed the weak interaction of CO with CaO(1 0 0) single crystals, but CO_2 is strongly bound to the surface. The carbonates appear to decompose into CO, as evident from multi-mass TDS; oxygen desorption has not been seen. The trends seen for S_0 are again consistent with predictions by a simple mass-match model. Accordingly, the S_0 of CO is systematically larger than the S_0 of CO_2.

5. Interaction of CO_2 with bimetallic surfaces–the case of Zn-on-Cu(1 1 0)

The formation of a brass surface alloy has been observed in studies about the MeOH synthesis reaction [3,92] on metal-oxide-based catalysts. Therefore, studying the effect of ZnCu surface alloys on adsorption processes more directly appears pertinent. In addition, the Zn-on-Cu system by itself can be regarded as a planar model catalyst since MeOH formation rates comparable with binary powder catalysts [92–94] have been determined. Interestingly, a maximum in the MeOH formation rate has been detected within a narrow Zn coverage range [95,96]. Furthermore, synergistic effects such as the formation of an intermediate bidentate formate species, adsorbed on Cu–Zn bridge sites, have been reported [93]. Bimetals, as model systems, also have the advantage that charged probe particles can be used without difficulties arising from changing the supports.

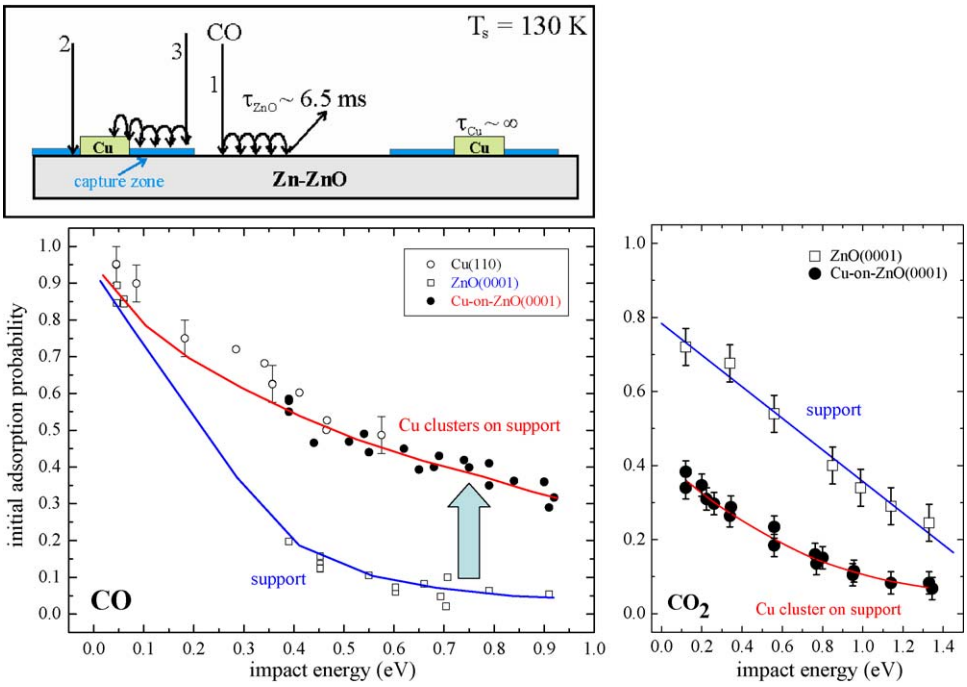

Fig. 9. (Top) Illustration of the capture zone model for supported metal nanoclusters. (Left) CO adsorption on clean ZnO(0 0 0 1) and Cu clusters supported on ZnO(0 0 0 1) [103,118]. (Right) CO_2 adsorption on the same systems [5,7,8,10].

The Zn-on-Cu(1 1 0) system also has been studied by molecular beam scattering techniques [11]. The main result here was a reduced CO_2 saturation coverage on the Cu(1 1 0) support when decorated with Zn. This result is surprising at a quick glance. Regarding the binding energies of CO_2 (Table 1), Zn clusters on a Cu(1 1 0) support should not block adsorption sites for CO_2 since the binding strength of CO_2 is stronger on zinc than on copper [5]. On the other hand, the formation of a surface alloy can affect the binding energies of probe molecules. This apparent (kinetic) "site blocking effect" indicates a lowering of the CO_2 binding energy on the alloyed surface compared with the clean Cu(1 1 0) support. Surface alloy formation on this system has also been confirmed in a MCS study [12].

6. Interaction of CO_2 with nanostructured surfaces

6.1. Probing the Cu-on-ZnO model catalyst by means of CO_2 adsorption

The growth morphology of Cu vapor deposited on ZnO(0 0 0 1) has literally been studied by all surface science techniques [97]. Agreement has been obtained [98,99] about the growth mode at small and large Cu coverage, Θ_{Cu}. Accordingly, 3D Cu clusters dominate the growth at large Θ_{Cu}, whereas 2D islands form at very low Θ_{Cu} [100]. If gas-phase species adsorb on this so-called model catalyst, the following elementary adsorption pathways are possible (Fig. 9). (1) Diffusion of the adsorbate along the bare support until it desorbs. (2) Direct adsorption of the probe on the metal deposits. (3) Diffusion along the support and capture of the probe molecule by the metal deposits.

The third possibility requires more attention and is typically discussed in the framework of the capture zone model. Even if the coverage of the probe molecule on the support is very small (e.g., 5×10^{-3} ML), its lifetime (surface residence time) can amount to several ms. Therefore, a large number of adsorption sites (e.g., $\sim 10^7$) can be sampled via surface diffusion before the adsorbate desorbs. Thus, even molecules that do not hit directly the metal deposits can diffuse along the support and adsorb on these high-energy binding sites. The blue squares in Fig. 9 indicate the so-called capture zone.[1] The capture zone is larger than the geometrical size of the deposits, leading in turn to an enhancement in S_0 compared with the values predicted by the ratio of the deposits to support areas.

The capture zone effect has indeed been observed for a variety of systems including CO adsorption on ZnO(0 0 0 1). Depositing very small amounts of Cu on the ZnO support increases S_0 distinctly compared with the clean support. In fact, 0.05 ML Cu are enough to raise S_0 to the values determined for a copper single crystal (Fig. 9 left-hand side). In contrast, this effect is absent when using CO_2 as the probe molecule (Fig. 9 right-hand side). The S_0 of CO_2 for Cu-on-ZnO(0 0 0 1) is systematically smaller than for the clean ZnO(0 0 0 1) support. Note that the S_0 of CO_2 on Cu single-crystal surfaces is also smaller than for ZnO(0 0 0 1). Therefore, in this case, an enhancement of S_0 for CO_2 by the Cu deposits cannot be expected. Considering, however, the small Cu coverage that already alters distinctly the support properties, a modification of the electronic properties of the support by the Cu deposits appears plausible. Indeed, some evidence for CO_2 adsorbing preferentially along the rim of the Cu clusters has been obtained [7,8].

For planar catalysts, molecular adsorption of small adsorbates such as CO_2 does not lead to a temperature dependence of S_0. However, effects of T_s on S_0 can be seen for model catalysts [101–103]. Both the surface residence time and the diffusion lifetime decrease with increasing T_s, i.e., the size of the capture zone should decrease as T_s increases. This leads to a predicted decrease in S_0 with T_s.

6.2. CO_2 adsorption on HOPG supported FeO_x nanoparticles

Iron oxide particles have been identified as a component of particulate matter in the plume of coal combustion plants, which may have serious implications for human health [104]. Thus, studying the adsorption of typical combustion gases appears

[1] For interpretation of the references to color in this sentence, the reader is referred to the web version of the article.

useful. Iron oxide clusters are complicated by the large number of different oxide phases [105] and their complex morphology [106,107]. In Refs. [24,25,108,109], iron was vapor deposited on HOPG and oxidized by annealing in O_2 to vary the oxidation state of the Fe-oxide clusters. Depending on the oxygen pretreatment, CO TDS curves consist of two peaks (indicating formation of γ-Fe_2O_3/Fe_3O_4) or one TDS peak (consistent with the dominance of α-Fe_2O_3 clusters). Thus, the oxidation state of Fe distinctly affects the adsorption kinetics of CO [109]. In CO_2 TDS data, three structures are seen, which are assigned to physisorbed CO_2 and carbonate decomposition. The adsorption dynamics of CO_2 and CO adsorption on FeO_x/HOPG have been characterized in Refs. [24,25,109] Due to size restrictions, only the references are given here.

6.3. CO_2 interaction with nanotubes—TiNTs and CNTs

The main application of TiNTs, which can be synthesized in the anatase or rutile polymorph as polycrystalline or amorphous NT, is in the field of photocatalysis [110]. The variety of different crystal structures while keeping the tubular structure of the nanotubes makes TiO_2 an attractive system to study a SAR. For example, we collected kinetics data for CO_2 adsorption [111]. The TDS data of CO_2 indicate systematically larger binding energies for the amorphous system. The width of the TDS peaks is large, indicating a number of kinetically distinct adsorption sites. By the way, the pore structure of coal may be approximated by CNTs, which have well-defined diameters. Despite the small binding energies of CO_2 on CNTs, the sorption (sequestration) capacity appears twice as large as for activated carbon [112,113]. For a detailed literature survey about UHV surface chemistry studies on NT, see Ref. [114].

7. Summary and conclusions

Carbon dioxide adsorption on 10 different systems, ranging from metal single crystals and metal oxides to nanostructured catalysts (Table 1), recently studied at NDSU by molecular beam scattering and kinetics techniques, has been considered. Some trends seen in our projects are briefly outlined in the following.

Kinetic SAR. A correlation of adsorption kinetics to structural features of surfaces has frequently been seen. Regarding metal oxides, oxygen vacancy sites lead typically to larger binding energies than adsorption on pristine sites and hence to a larger concentration of reactants on the surface (“The bad sites—defects—are the good sites”). Thus, a kinetic structure activity relationship (SAR) is present for CO_2 adsorption on ZnO, TiO_2, and CaO.

Dynamic SAR, S_0. The effect of surface defects on the gas-surface energy transfer processes (dynamic SAR) has not been addressed very often. Indeed, the variations in the initial adsorption probability, S_0, with defect density, are typically rather small. Whereas binding energies for CO_2 increase, the S_0 of CO_2 appears to decrease with increasing defect density. (“Adsorption kinetics and dynamics are not necessarily directly correlated.”)

Dynamic SAR, $S(\Theta)$. Interestingly, the shape of $S(\Theta)$ curves is more distinctly affected by the presence of defects than S_0. In particular, the (“autocatalytic”) adsorbate-assisted adsorption effect is weakened by defects, strong surface corrugation, and the parallel momentum component of the gas-phase species. Typically an energy threshold is seen, which suggests a dynamic effect rather than the influence of lateral interactions. (“The shape of $S(\Theta)$ is a very sensitive indicator of surface defects.”)

Mass-match models. Some molecular beam scattering results are in agreement with simple mass-matching considerations. For example, S_0 (at the same impact parameters) of CO on Zn-ZnO, S_0(CO/Zn), is smaller than for O-ZnO (S_0(CO/Zn) < S_0(CO/O)) and S_0(CO_2/Zn) > S_0(CO/Zn) for Zn–ZnO. Similar trends are evident for Cr and Cr-oxides. (“As a very simple rule of thumb, the better the mass match, the larger S_0.”)

Capture zone effect. Metal clusters lead to an enhancement in S_0 that is larger than expected from the geometric size of the metal deposits. This hold true, as long as the metal is more reactive than the support. However, details about the temperature dependence and shape of $S(\Theta)$ are not always consistent with simple capture zone models.

Reactivity trends. Unexpectedly, even alkanes decompose on CaO as well as carbonates form efficiently. Indeed, theoretical studies predict great catalytic activity of alkaline-earth oxides. Accordingly, a higher activity of CaO compared with, for example, MgO, is related to a lower Madelung potential, which leads to a more delocalized electron distribution of surface oxygen. Therefore, a more efficient overlap with the orbitals of adsorbing molecules becomes possible. (“Along the alkaline-earth oxide series reactivity may scale with variations in the lattice constant.”)

Acknowledgements

Most of the projects summarized here were part of the thesis work of S. Funk [115] and J. Goering [116] as well as the work of postdocs J. Wang and E. Kadossov at North Dakota State University. This short review also includes some work done with P. Schmuki’s group at Erlangen-Nuerberg University on TiO_2 nanotubes. Financial support from the Chemical Sciences, Geosciences, and Biosciences Division, Office of Basic Energy Sciences, Office of Science, U.S. Department of Energy is acknowledged (DE-FG02-08ER15987) as well as by NSF CAREER (CHE-0743932).

References

[1] J.T. Yates, Surf. Sci. 299/300 +(1994) 731.
[2] J.B. Hansen, in: G. Ertl, H. Knötzinger, J. Weitkamp (Eds.), Ch. 3.5: Methanol Synthesis in Handbook of Heterogeneous Catalysis, +VCH, 2001.
[3] T.S. Askgaard, J.K. Norskov, C.V. Ovesen, P. Stoltze, J. Catal. 156 +(1995) 229.
[4] G.A. Olah, A. Goeppert, G.K.S. Prakash, Beyond Oil and Gas: The Methanol Economy, + Wiley-VCH, 2003, ISBN: 0-471-41782-3.
[5] J. Wang, U. Burghaus, J. Chem. Phys. 122 +(2005) 044705.
[6] J. Wang, B. Hokkanen, U. Burghaus, Surf. Sci. 577 +(2005) 158.
[7] J. Wang, S. Funk, U. Burghaus, Catal. Lett. 103 +(2005) 219.
[8] J. Wang, S. Funk, U. Burghaus, J. Chem. Phys. 123 +(2005) 204710.
[9] J. Wang, U. Burghaus, Chem. Phys. Lett. 403 +(2005) 42.
[10] J. Wang, U. Burghaus, Surf. Rev. Lett. 11 +(2004) 521.
[11] S. Funk, B. Hokkanen, J. Wang, U. Burghaus, G.H. Bozzolo, J.E. Garcès, Surf. Sci. 600 +(2005) 1870.
[12] S. Funk, G.H. Bozzolo, J.E. Garces, U. Burghaus, Surf. Sci. 600 +(2005) 195.
[13] S. Funk, B. Hokkanen, J. Wang, U. Burghaus, G.H. Bozzolo, J.E. Garces, Surf. Sci. 600 +(2006) 583.
[14] L. Marini, Geological Sequestration of Carbon Dioxide in Developments in Geochemistry, vol. 11, +Elsevier, 2007 ISBN-13 978-0-444-52950-3.
[15] E. Kadossov, U. Burghaus, J. Phys. Chem. C 112 +(2008) 7390.
[16] D. Cazoria-Amoros, J.P. Joly, A. Linares-Salano, A. Marcilla-Gomis, C.S.M. Lecea, J. Phys. Chem. 95 +(1991) 6611.
[17] A.L. Solano, M.A. Alarcon, S.S.M. Lecea, J. Catal. 125 +(1990) 401.
[18] C.H. Lin, T. Ito, J. Wang, H.J. Lunsford, J. Am. Chem. Soc. 109 +(1987) 4808.
[19] F. Acke, I. Panas, J. Phys. Chem. B 102 +(1998) 5127.
[20] O.B. Koper, E.A. Wovchko, J.A. Glass, J.T. Yates, K.J. Klabunde, Langmuir 11 +(1995) 2054.
[21] A. Snis, I. Panas, Surf. Sci. 412/413 +(1998) 477.
[22] S. Funk, U. Burghaus, Phys. Chem. Chem. Phys. 8 +(2006) 4805.
[23] S. Funk, B. Hokkanen, E. Johnson, U. Burghaus, Chem. Phys. Lett. 422 +(2006) 461.
[24] E. Kadossov, U. Burghaus, Surf. Int. Anal. 40 +(2008) 893.
[25] E. Kadossov, U. Burghaus, M.R. Hoffmann, Am. Chem. Soc., Div. Fuel Chem. 53 +(2008) 855.
[26] S. Funk, T. Nurkic, B. Hokkanen, U. Burghaus, Appl. Surf. Sci. 253 +(2007) 7108.
[27] F. Solymosi, J. Mol. Catal. 65 +(1991) 337.
[28] H.J. Freund, M.W. Roberts, Surf. Sci. Rep. 25 +(1996) 225.
[29] M. Aresta, A. Dibenedetto, Dalton Trans. 2975 +(2007) 2975.
[30] C. Song, Catal. Today 115 +(2006) 2.
[31] T. Sakakura, J. Choi, H. Yasuda, Chem. Rev. 107 +(2009) 2365.
[32] G. Scoles, in: G. Scoles (Ed.), Atomic and Molecular Beam Methods, +Oxford University Press, 1988.
[33] J.W. Niemantsverdriet, K. Markert, K. Wandelt, Appl. Surf. Sci. 31 +(1988) 211.
[34] K.H. Ernst, D. Schlatterbeck, K. Christmann, Phys. Chem. Chem. Phys. 1 +(1999) 4105.

[35] P.B. Rasmussen, P.A. Taylor, I. Chorkendorff, Surf. Sci. 269/270 +(1992) 352.
[36] X. Ding, L.D. Rogatis, E. Vesselli, A. Baraldi, G. Comelli, R. Rosei, L. Savio, L. Vattuone, M. Rocca, P. Fornasiero, F. Ancilotto, A. Baldereschi, M. Peressi, Phys. Rev. B 76 +(2007) 195425.
[37] S.S. Fu, G.A. Somorjai, Surf. Sci. 262 +(1992) 68.
[38] G.C. Wang, L. Jiang, Y. Morikawa, J. Nakamura, Z.S. Cai, Y.M. Pan, X.Z. Zhao, Surf. Sci. 570 +(2004) 205.
[39] S. Kneitz, J. Gemeinhardt, H. Koschel, G. Held, H.P. Steinrück, Surf. Sci. 433 +(1999) 27.
[40] S. Kneitz, J. Gemeinhardt, H.P. Steinrück, Surf. Sci. 440 +(1999) 307.
[41] H.P. Steinrück, R.J. Madix, Surf. Sci. 185 +(1987) 36.
[42] M. Kunat, C. Boas, T. Becker, U. Burghaus, C. Wöll, Surf. Sci. 474 +(2001) 114.
[43] U. Burghaus, H. Conrad, Surf. Sci. 331 +(1995) 116.
[44] U. Burghaus, J. Ding, W.H. Weinberg, Surf. Sci. 396 +(1998) 273.
[45] C.L. Kao, A. Carlsson, R.J. Madix, Surf. Sci. 497 +(2002) 356.
[46] G. Hes, C. Baumgartner, A. Petkova, H. Froitzheim, Surf. Sci. 572 +(2004) 355.
[47] O. Seiferth, K. Wolter, B. Dillmann, G. Klivenyi, H.J. Freund, D. Scarano, A. Zecchina, Surf. Sci. 421 +(1999) 176.
[48] U. Burghaus, Trends in Physical Chemistry 8 +(2001) 21.
[49] C.L. Kao, R.J. Madix, Surf. Sci. 557 +(2004) 215.
[50] C. Kao, A. Carlsson, R.J. Madix, Surf. Sci. 565 +(2004) 70.
[51] U. Burghaus, J. Stephan, J.M. Rogowska, L. Vattuone, A Practical Guide to Monte Carlo Simulations and Classical Molecular Dynamics Simulation—An Example Book, + NOVA Science, New York, US, 2006, ISBN: 1-59454-531-6.
[52] U. Diebold, Surf. Sci. Rep. 48 +(2003) 1.
[53] W. Göpel, G. Rocker, R. Feierabend, Phys. Rev. B 28 +(1983) 3427.
[54] T.L. Thompson, O. Diwald, J.T. Yates, J. Phys. Chem. 107 +(2003) 11700.
[55] M.A. Henderson, Surf. Sci. 400 +(1998) 203.
[56] M.A. Henderson, Surf. Sci. 419 +(1999) 174.
[57] V.E. Henrich, G. Dresselhaus, H.J. Zeiger, Phys. Rev. Lett. 36 +(1976) 1335.
[58] C.N. Rusu, J.T. Yates, Langmuir 13 +(1997) 4311.
[59] Q. Zhong, J.M. Vohs, D.A. Bonnell, Surf. Sci. 274 +(1992) 35.
[60] S.A. French, A.A. Sokol, S.T. Bromley, C.R.A. Catlow, S.C. Rogers, F. King, P. Sherwood (Eds.), Angew. Chem. Int. 40 +(2001) 4437.
[61] S. Wendt, R. Schaub, J. Matthiesen, E.K. Vestergaard, E. Wahlström, M.D. Rasmussen, P. Thostrup, L.M. Molina, E. Lægsgaard, I. Stensgaard, F. Besenbacher, Surf. Sci. 598 +(2005) 226.
[62] V. Staemmler, K. Fink, B. Meyer, D. Marx, M. Kunat, S.G. Girol, U. Burghaus, C. Wöll, Phys. Rev. Lett. 90 +(2003) 106102.
[63] O. Dulub, L.A. Boatner, U. Diebold, Surf. Sci. 519 +(2002) 201.
[64] O. Dulub, U. Diebold, G. Kresse, Phys. Rev. Lett. 90 +(2003) 016102.
[65] M. Kunat, S.G. Girol, U. Burghaus, C. Wöll, J. Phys. Chem. 6 +(2004) 4203.
[66] M. Kunat, S. Gil-Girol, T. Becker, U. Burghaus, C. Wöll, Phys. Rev. B 66 +(2002) 081402(R).
[67] T. Becker, S. Hövel, C. Boas, M. Kunat, U. Burghaus, C. Wöll, Surf. Sci. 486 +(2001) L502.
[68] P.J. Moller, S.A. Komolov, E.F. Lazneva, E.H. Pedersen, Surf. Sci. 323 +(1995) 102.
[69] W. Hotan, W. Göpel, R. Haul, Surf. Sci. 83 +(1979) 162.
[70] J.B. Martins, E. Longo, C.A. Taft, Int. J. Quant. Chem. 70 +(1998) 367.
[71] W. Goepel, R.S. Bauer, G. Hansson, Surf. Sci. 99 +(1980) 138.
[72] W.H. Cheng, H.H. Kung, Surf. Sci. 122 +(1982) 21.
[73] S.F. Jen, A.B. Anderson, Surf. Sci. 223 +(1989) 119.
[74] P. Esser, W. Göpel, Surf. Sci. 97 +(1980) 309.
[75] B. Poelsema, G. Comsa, Scattering of Thermal Energy Atoms from Disordered Surfaces, vol. 115, + Springer Tracts in Modern Physics, Springer, 1989.
[76] U. Burghaus, Res. Trends Phys. Chem. 11 +(2006) 1.
[77] U. Burghaus, Surf. Rev. Lett. 8 +(2001) 353.
[78] J. Stephan, U. Burghaus, Surf. Sci. 507–510 +(2002) 736.
[79] J. Stephan, U. Burghaus, J. Vac. Sci. Technol. A21 +(2003) 1284.
[80] E. Kadossov, U. Burghaus, Chem. Commun. +(2008) 4073.
[81] L. Vattuone, U. Burghaus, U. Valbusa, M. Rocca, Surf. Sci. 408 +(1998) L693.
[82] M.C. McMaster, R.J. Madix, J. Chem. Phys. 98 +(1993) 9963.
[83] G.R. Darling, S. Holloway, Rep. Prog. Phys. 58 +(1995) 1595.
[84] M. Kunat, U. Burghaus, Surf. Sci. 544 +(2003) 170.
[85] C.S. Doyle, T. Kendelewicz, X. Carrier, G.E. Brown, Surf. Rev. Lett. 6 +(1999) 1247.
[86] D. Ochs, B. Braun, W. Maus-Friedrichs, V. Kempter, Surf. Sci. 417 +(1998) 406.
[87] F. Voigts, F. Bebensee, S. Dahle, K. Volgmann, W. Maus-Friedrichs, Surf. Sci. 603 +(2009) 40.
[88] D. Beruto, R. Botter, A.W. Searcy, J. Phys. Chem. 88 +(1984) 4052.
[89] Y. Fukuda, K. Tanabe, Bull. Chem. Soc. Jpn. 46 +(1973) 1616.
[90] G. Pacchioni, J.M. Ricart, F. Illas, J. Am. Chem. Soc. 116 +(1994) 10152.
[91] M.B. Jensen, L.G.M. Pettersson, O. Swang, U. Olsbye, J. Phys. Chem. B 109 +(2005) 16774.
[92] I. Nakamura, T. Fujitani, T. Uchijima, J. Nakamura, J. Vac. Sci. Technol. A 14 +(1996) 1464.
[93] J. Nakamura, I. Nakamura, T. Uchijima, Y. Kanai, T. Watanabe, M. Saito, T. Fujitani, J. Catal. 160 +(1996) 65.
[94] T. Fujitani, I. Nakamura, T. Uchijima, J. Nakamura, Surf. Sci. 383 +(1997) 285.
[95] M. Haruta, Catal. Today 36 +(1997) 153.
[96] M. Haruta, B.S. Uphade, S. Tsubota, A. Miyamoto, Res. Chem. Intermed. 24 +(1998) 329.
[97] C.T. Campbell, Surf. Sci. Rep. 27 +(1997) 1.
[98] G. Kresse, O. Dulub, U. Diebold, Phys. Rev. B 68 +(2003) 245409.
[99] J. Yoshihara, J.M. Campbell, C.T. Campbell, Surf. Sci. 406 +(1998) 235.
[100] L.V. Koplitz, O. Dulub, U. Diebold, J. Phys. Chem. 107 +(2003) 10583.
[101] C.R. Henry, Surf. Sci. Rep. 31 +(1998) 235.
[102] T. Schalow, B. Brandt, M. Laurin, S. Schauermann, S. Guimond, H. Kuhlenbeck, J. Libuda, H.J. Freund, Surf. Sci. 600 +(2006) 2528.
[103] J. Wang, U. Burghaus, J. Chem. Phys. 123 +(2005) 184716.
[104] W.S. Seames, Fuel Process. Technol. 81 +(2003) 109.
[105] W. Weiss, W. Ranke, Prog. Surf. Sci. 70 +(2002) 1.
[106] C.M. Wang, D.R. Baer, J.E. Amonette, M.H. Engelhard, Y. Qiang, J. Antony, Nanotechnology 18 +(2007) 255603.
[107] C.M. Wang, D.R. Baer, L.E. Thomas, J.E. Amonette, J. Appl. Phys. 98 +(2005) 094308.
[108] E. Kadossov, J. Goering, U. Burghaus, Surf. Sci. 602 +(2008) 811.
[109] E. Kadossov, S. Funk, U. Burghaus, Catal. Lett. 120 +(2007) 179.
[110] S. Funk, B. Hokkanen, U. Burghaus, A. Ghicov, P. Schmuki, Nano Lett. 7 +(2007) 1091.
[111] S. Funk, B. Hokkanen, T. Nurkic, J. Goering, E. Kadossov, U. Burghaus, A. Ghicov, P. Schmuki, Z.Q. Yu, S. Thevuthasan, L.V. Saraf, ACS Symposium Series 996, +Oxford Uni. Press, Chicago, 2007, ISBN: 978-0-8412-6969-9.
[112] L. Huang, L. Zhang, Q. Shao, L. Lu, X. Lu, S. Jiang, W. Shen, J. Phys. Chem. C 111 +(2007) 11912.
[113] A.I. Skoulidas, D.S. Sholl, J.K. Johnson, J. Chem. Phys. 124 +(2006) 054708.
[114] U. Burghaus, Gas-carbon Nanotubes Interactions: A Review of Ultra-High Vacuum Surface Science Studies on CNTs in Carbon Nanotubes—Research Trends, + Nova Science, New York, 2009, ISBN: 978-1-60692-236-1.
[115] S. Funk, Ph.D. Thesis, North Dakota State University, 2007.
[116] J. Goering, Masters Thesis, North Dakota State University, 2008.
[117] J.B. Hansen, Handbook of Heterogeneous Catalysis, vol. 1, + VCH, 1997.
[118] J. Wang, E. Johnson, U. Burghaus, Chem. Phys. Lett. 410 +(2005) 131.
[119] E. Kadossov, M.R. Hoffmann, U. Burghaus, Am. Chem. Soc., Div. Fuel Chem. 54 +(2009) 268.